XXVI International Mineral Processing Congress (IMPC 2012)

Influence of particle shape and roughness on the induction period for particle–bubble attachment

D. I. Verrelli,[*] W. J. Bruckard, P. T. L. Koh, M. P. Schwarz and B. Follink

Paper Reference Number: 317

Preferred presentation format: Oral presentation

Corresponding Author

Title	Dr.
First Name	David
Middle Name / Initial	I.
Last Name / Surname	Verrelli
Affiliation (Institute / Organization)	CSIRO Process Science and Engineering
Address Line1	Bayview Avenue
Address Line2	
City	Clayton, Victoria
Zip Code	3168
Country	Australia
Email Address	David.Verrelli@csiro.au
Telephone	(+613)-9545-8689
Mobile	N/A

Presenting Author

Title	Mr.
First Name	Warren
Middle Name / Initial	J.
Last Name / Surname	Bruckard
Affiliation (Institute / Organization)	CSIRO Process Science and Engineering
Address Line1	Bayview Avenue
Address Line2	
City	Clayton, Victoria
Zip Code	3168
Country	Australia
Email Address	Warren.Bruckard@csiro.au
Telephone	(+613)-9545-8566
Mobile	N/A

Influence of particle shape and roughness on the induction period for particle–bubble attachment

David I. Verrelli[*1], *Warren J. Bruckard*[1], *Peter T. L. Koh*[2], *M. Philip Schwarz*[2] *and Bart Follink*[3]

1.
CSIRO Process Science and Engineering, Bayview Avenue, Clayton, VIC 3168, Australia. Email: David.Verrelli@csiro.au ; Warren.Bruckard@csiro.au

2.
CSIRO Mathematics, Informatics and Statistics, Bayview Avenue, Clayton, VIC 3168, Australia. Email: Peter.Koh@csiro.au ; Phil.Schwarz@csiro.au

3.
Global Research Alliance, 343 Royal Parade, Parkville, VIC 3052, Australia. Email: Bart.Follink@csiro.au

ABSTRACT

Within the flotation community a belief has developed that some particle shapes are more 'floatable' than others. This is usually attributed to an influence of particle shape or roughness on the induction period required to achieve attachment between the particles and the air bubbles in the pulp. Up to now such measurements have not been able to readily isolate the effect on individual flotation subprocesses. In contrast, our experimental apparatus, the *CSIRO Milli-Timer*, enables us to directly observe the process of particle–bubble interaction and attachment by means of a high-speed video recording, thus providing a direct measure of the induction period for attachment.

To assess the influence of particle shape on induction time we used two varieties of methylated borosilicate glass particles — spheres and angular 'frit' — in a range of tightly-sized fractions. In doing this we take care to account for the influence of other factors that could affect the induction time, such as the polar angle of sliding commencement, and approach velocity. These parameters are recorded as variables for each interaction, and corrected for using multiple nonlinear regression.

Our results illustrate the importance of particle shape on induction period, with angular particles exhibiting induction periods that were an order of magnitude lower than those of spheres. Furthermore, the induction period was seen to decrease with increasing particle velocity, or kinetic energy on approach, but increased as the trajectory approached the limit of just grazing the bubble.

Particle shape in mineral processing is a consequence chiefly of the mineral type and the type of grinding employed. The results presented herein indicate that attention should be paid to the *shape* of particles obtained from the grinding operation, besides particle *size*.

Keywords: attachment; bubbles; flotation; induction period; particles; shape effects; surface roughness

INTRODUCTION

Flotation is a key unit operation employed in mineral processing and a range of other industries. Successful flotation hinges on the attachment of (certain) particles to bubbles. In real industrial systems the mineral particles fed into a flotation cell will exhibit a variety of shapes, varying from approximately spherical (*e.g.* zircon), to cuboidal (*e.g.* galena) (Dippenaar, 1982), to platy (*e.g.* talc, chlorite) or acicular (*e.g.* tremolite) (Kursun and Ulusoy, 2006). How important is this shape in determining attachment?

Anecdotally it is expected that particle shape can have a significant effect on 'floatability': the common view is that angular particles are easier to float than rounder particles. However, such overall tendencies leave it unclear as to which flotation sub-processes are most affected by particle shape. For example, in the pulp we could consider collision rate, attachment efficiency, stability against detachment, and entrainment, besides a number of froth characteristics. Traditionally the efforts to model the interaction of particles and bubbles have typically assumed that both objects are perfect spheres (see Nguyen and Schulze, 2004). Some exceptions are studies on the final moments prior to breaching of the liquid gap, in which bubble deformation is modelled (Chan, Klaseboer and Manica, 2011), and studies that examine the equilibrium configuration of

the particle *after* attachment has occurred in the pulp (Huh and Mason, 1974; Schulze, 1984: 199ff.) or the froth (Dippenaar, 1982; Morris, Neethling and Cilliers, 2011). Hence, modelling is not yet at a stage to fully explain the relative importance of particle shape or roughness.

Influences on particle shape, and roughness

A number of studies have been reported in the literature in which the effects of different grinding processes on a given sample are reported. A typical result is that more angular particles are produced from rod mills (attributed to impact processes), compared to rounder particles obtained from ball mills (attributed to abrasion and chipping) (Yekeler, Ulusoy and Hiçyılmaz, 2004), although this depends on the details of operation (Gaudin, 1926). Yet at the same time the particles ground in a rod mill have been reported to be smoother than particles from a ball mill (Yekeler, Ulusoy and Hiçyılmaz, 2004). Autogenous milling reportedly produced intermediate results in each parameter (Yekeler, Ulusoy and Hiçyılmaz, 2004). Dry and wet milling was carefully studied by Feng & Aldrich (2000), who found that the dry-ground particles had relatively rough surfaces containing microstructural defects, whereas the wet-ground particles had smoother, cleaner surfaces.

Other important factors are discussed *inter alia* by Gaudin (1926) and Holt (1981).

Effect on flotation

Shape

One of the key resistances to attachment is the hydrodynamic resistance arising as liquid drains out of the gap between a bubble and an approaching particle. Aspherical particles could experience a lower resistance (depending upon their shape and orientation), and hence require less time for the intervening gap to thin sufficiently to be breached, and attachment occur.

There have been few systematic studies on the effect of particle shape or roughness upon flotation performance. Ahmed (2010) has recently reviewed the literature in this area. In distilled water, Anfruns & Kitchener (1977) found collection efficiencies about four times greater for angular quartz than for spherical glass particles. Studies on talc have suggested that rounder (but rougher) particles produced by ball milling are less easily recovered in a microflotation cell (Yekeler, Ulusoy and Hiçyılmaz, 2004) and in column flotation (Kursun and Ulusoy, 2006), compared to more elongated (but smoother) particles produced by rod milling. Finally, Ahmed's work showed increases in flotation recovery — and greater resistance to detachment — with increases in either particle asphericity or particle roughness (Ahmed, 2010).

Roughness

Particles with rough surfaces composed of microscale projections might achieve attachment more easily, if those bumps or jags protrude through the gap, so that the separation between particle and bubble is smaller than it might otherwise seem. A three-phase contact would then be expected to occur on one of the projections. Nanoscale topological features seem less likely to have much effect on the ease of breaching the interjacent liquid; however, they may still affect the expansion of the three-phase contact line in

dewetting (Oliver and Mason, 1977). Moreover, chemical composition and surface properties can vary on the atomic scale in layered crystalline materials (Yekeler, Ulusoy and Hiçyılmaz, 2004; Franks and Gan, 2007), which would be accentuated on rough surfaces. A further feature of rough surfaces is that they may more readily harbour small air bubbles ('microbubbles' or 'nanobubbles'), which promote attachment by some mechanism — possibly including 'hydrophobic forces' (Krasowska *et al.*, 2007).

Feng & Aldrich (2000) found a large number of differences in the particles prepared by wet and dry milling, with the dry-ground samples exhibiting faster dissolution, faster reagent adsorption, more stable and higher-loaded froths, and faster flotation kinetics.

Complicating factors

Different grinding techniques do not just affect the physical form of the minerals, but can also affect the chemistry of the surface, for example through more or less reducing conditions (Forssberg, Sundberg and Hongxin, 1988; Bruckard, Sparrow and Woodcock, 2011), and "activation" of the mineral surface through creation of material defects or disorder (Feng and Aldrich, 2000; Yekeler, Ulusoy and Hiçyılmaz, 2004).

Induction period

The attachment between a bubble and a particle (**Figure 1**) is commonly described as requiring a minimum, 'critical' time to occur, once the two bodies are brought into proximity; this is the induction period, τ (Sven-Nilsson, 1934). In flotation, the conventional theory compares τ against the time available for a particle to slide over the bubble's surface (Nguyen and Schulze, 2004: 265ff.). Based on hydrodynamics, the sliding time is known to depend upon factors such as particle size, and the approach trajectory. The induction period is expected to depend on the surface chemistry, and perhaps other factors such as particle shape. For a given particle and bubble pair, the induction period is tacitly presumed to be constant; however, the latest research indicates that τ actually depends upon the particle's approach trajectory (Verrelli *et al.*, 2012).

We are interested in using our technique of direct observation of the induction period in order to assess the role of the attachment process in the previously reported changes in floatability. This will establish whether the altered floatability is due to changes in the ease of attachment, following from changes in the time required for thinning of the interposed liquid, or whether it is due to other factors, such as detachment or entrainment.

In order to assess the importance of particle shape and roughness on the induction period, τ, it is necessary to account for as many other factors as possible. Hence, we conduct our experiments on narrowly sized borosilicate glass particles that differ only in their shape and surface roughness. We are unable to precisely control the particle approach trajectories or speeds, so instead we include corrections for these parameters in the analysis.

METHODOLOGY

CSIRO Milli-Timer

The *CSIRO Milli-Timer* (**Figure 2**) has been described in detail previously (Verrelli, Koh and Nguyen, 2011). Briefly, it consists of a stationary bubble that is held underwater at the end of a capillary, and onto which particles are dropped. The interactions are recorded on a high-speed video camera.

In the present set-up the camera used was a *Phantom v210* (Vision Research, Wayne, U.S.A.), fitted with a *Zoom 6000* lens assembly (Navitar, Rochester, U.S.A.) comprising a 2× magnifying F-mount extension tube, a zoom lens with focussing capability, and a 0.75× lens attachment, for a nominal magnification of 6.75× through the lens assembly. The actual magnification of the camera–lens system is approximately 7.1×. The camera was operated at a capture rate of 1000 frames per second, and exposure time of 10 µs.

A *KL 1500 LCD* 150 W halogen cold light source (Schott, Mainz, Germany) provides intense white light. To minimise image blur due to differential refraction of different wavelengths of light, a *BP635* colour filter (Midwest Optical Systems) was interposed, which passes wavelengths in the range 590–670 nm.

Induction periods are defined as the time that elapses from the moment at which sliding commences, until the moment that attachment is initiated (see **Figure 1**). The latter is clearly evidenced by a 'jump in' event, as described previously (Verrelli and Koh, 2010; Verrelli, Koh and Nguyen, 2011). The former requires some judgement. In the ideal case, the particle will approach the bubble and then undergo sliding within the plane perpendicular to the camera's viewing axis and passing through the bubble's centre (*i.e*. approximately the middle of the focal 'plane'). In reality the particles are commonly observed to travel along slightly deviating azimuthal angles (Verrelli *et al.*, 2012), so that it is more practical to determine sliding commencement by identifying a substantial reduction in the radial velocity of the particle with respect to the bubble's centre.

Materials

Bubbles

Bubbles of 2.0 µL volume were blown at the end of a blunt 20 gauge capillary shortly before each run using ambient air, giving diameters of 1.56±0.04 mm.

Particles

The particles used were composed of borosilicate glass, in two forms: spheres, and angular 'frit' (Mo-Sci Specialty Products, Rolla, U.S.A.). The spheres were supplied in a 75–90 µm size fraction, designated as "Precision Grade", which are specified as being at least 90 % in the nominated size range and at least 90 % classed as "spherical". The scanning electron microscope (SEM) images we have taken in **Figure 3(A)** confirm a narrow size distribution, and high sphericity, with rather smooth surfaces. The frit is manufactured by comminution of large chunks of recycled borosilicate glass, first in a hammer mill, and then in a disk mill (*e.g*. *Bico* plate pulveriser). SEM images of the frit in **Figure 3(B)** show the variety of shapes encountered. Using new screens, we sieved the as-received frit into narrow size fractions, of which the 75–90 µm fraction was used in the present work.

All particles were washed using progressive stages of water rinsing, alkaline washing and acid washing (Verrelli *et al.*, 2012). The clean particles were then methylated using chloro(trimethyl)silane (CTMS) to achieve a surface coverage equal to 50 % of the maximum achievable coverage (Verrelli *et al.*, 2012), designated as "50 % methylated". This process increases particle hydrophobicity by adsorption of a stable coating on the particle.

Characterisation of particles

The specific surface area of the frit was characterised using the approach suggested by Brunauer, Emmett & Teller (1938). Measurements were attempted first using a *TriStar 3000* surface area analyser (Micromeritics, Atlanta, U.S.A.) operating with nitrogen gas, with sample masses between 0.6 and 0.7 g. However, this proved inadequate for the small surface areas involved. Hence, final characterisation was carried out on a *TriStar II 3020* (Micromeritics), operating with argon gas for improved sensitivity, with sample masses between 1 and 2 g. Confidence intervals on each measurement were evaluated based on uncertainty in the regression (including covariance (Montgomery, Peck and Vining, 2001: 32,74,82f.,103f.)); it does not include errors from other sources.

Micrographs were taken with a field emission, environmental SEM (FEI, Oregon, U.S.A.) operating at 10 kV and a probe current of approximately 300 pA.

Multiple nonlinear regression

In order to systematically investigate the influence of three key mechanisms on induction period, rigorous statistical analysis was performed in the form of multiple nonlinear regression. The three key issues explored are the effect of approach velocity, approach position, and particle shape or roughness. These are described by the approach velocity, v_0, the polar angle of sliding commencement, φ^*, and a binary "indicator variable", f, that takes a value of either 1 for frit or 0 for spheres.

We performed the regression using the following general equation:

$$\tau = \left(\beta_1 \frac{1}{{v_0}^{10}} + \beta_2 \frac{1}{{v_0}^2} + \beta_3 \frac{1}{v_0} + \beta_4 v_0 + \beta_5 {v_0}^2 + \beta_6 \varphi + \beta_7 \varphi^2 + \beta_8 \cos(\varphi) + \beta_9 \right) \left(\beta_{10} f + (1-f) \right), \quad (1)$$

in which the β_i are constant coefficients. We evaluated equation 1 for the set of all possible regressions (Montgomery, Peck and Vining, 2001: 302ff.). The 'best' regression for a given number of parameters was that which minimised the mean squared error ("MSE").

* This was given the symbol φ_1 in our previous publication (Verrelli *et al.*, 2012). The subscript is omitted here for clarity.

RESULTS AND DISCUSSION

Particle shape, and roughness

The nominally spherical particles are seen in **Figure 3(A)** to mostly approximate ideal spheres. They do, however, exhibit some roughness due to 'debris' melded on their surfaces. This debris is of irregular shape, but of size approximately 0.1 to 5 μm, and is composed of the parent material. A small number of angular particles are seen intermingled in **Figure 3(A)(i)**; those angular particles are readily discerned on the video recording, and are excluded from further analysis.

The frit used in the present experiments was produced by comminution in a hammer mill and disk mill in sequence. It would be expected that the final particle shape and roughness would be influenced more by the later stage. Particle size reduction in disk mills is due principally to shear, with smaller contributions from particle compression, impact and other mechanisms, which is not so different from the hammer mill (Austin and Rogers, 1985). The few previous reports on disk mills in the literature (Husemann, Bernhardt and Heegn, 1976; Ofori-Sarpong and Amankwah, 2011) are not directly relevant, due to the different materials used.

Arguably the most straightforward means of classification is still human 'intuition' (cf. Ahmed, 2010). Micrographs of the frit are presented in **Figure 3(B)**. It is apparent that the most common shapes are platy fragments, although other shapes are also observed, such as tetrahedra and cuboids. As with the spherical particles, the frit exhibits roughness due to 'debris' of size approximately 0.1 to 5 μm stuck on the surface. In addition to this, step-like features, cavities, ridges, grooves and so forth can be seen in the substrate, of a similar dimension.

Surface area

The specific surface area provides a quantitative measure. Experimental results are given in **Figure 4**. For the spheres the BET surface area was found to be approximately 0.0365 m^2/g, which is close to the expected value for a perfect sphere. For frit of the same nominal size fraction the surface area was 0.0614 m^2/g. This represents a ratio of 1/1.68 = 0.59, which can be interpreted as a sphericity-like measure (Koh *et al.*, 2009), although conventionally the sphericity is defined as relating particles of equal volume (Wadell, 1935: 264), rather than equal size fraction. Recognising the uncertainty in estimating the small surface area of the spherical particles, and recalculating the ratio using the lower limit of the confidence interval or the theoretically expected value for ideal spheres (which happen to be approximately equal here) the ratio becomes 1/1.85 = 0.54. Although in the present work only particles in a single size fraction were used, namely 75–90 μm, the BET data indicates that particle asphericity increases as the particle size decreases; this is consistent with previous reports (Gaudin, 1926; Holt, 1981).

Measured reagent consumption for the borosilicate spheres at 100 % methylation indicates chemisorption of 10 mg/m^2 of pure CTMS, assumed independent of particle size[*], after correcting for reagent degradation and

[*] In this calculation the surface area is estimated using the mid-range particle size.

losses (Verrelli *et al.*, 2012). The same consumption is obtained for borosilicate frit when its specific surface area is taken as 2.0 times the specific surface area of spherical particles in the same size fraction, implying a ratio of specific surface areas equal to 0.50. (For the soda–lime glass *Ballotini* used previously, 18.5 mg/m^2 of CTMS was consumed for full methylation (Verrelli *et al.*, 2012). The same level of consumption applied also to ground *Ballotini* (Verrelli *et al.*, 2012), when its surface area was taken as being 1/0.41 = 2.44 times greater than that of an ideal sphere in the same size fraction, as suggested by BET surface area measurements (Koh *et al.*, 2009).)

Induction period for attachment

In **Figure 5** and **Figure 6** induction period results are presented for spheres and frit, respectively. We have previously described a theoretical rationale for the induction period to depend upon the polar angle at which the particle impinges on the bubble (Verrelli *et al.*, 2012). Furthermore, models of the attachment process commonly posit that the attachment will be easier for particles approaching at higher velocities (*i.e.* greater kinetic energy) (Yoon and Luttrell, 1989; Yoon and Mao, 1996; Nguyen and Schulze, 2004: 265,268). Both of these influences are depicted in the graphs.

It should be noted that in the case of angular particles much greater variation in the results can be expected as a consequence of the anticipated dependence on the orientation of the impinging particle. For example, a cubic particle could impinge point-first or face-on. The hydrodynamic resistances will assuredly be different, the relationship between gap and surface forces will be different, and even the surface chemistry may be different, so a different induction period could also be expected. However, as seen from the SEM images, the frit exists in a wide range of shapes, so that a simple quantification of the impinging particle's orientation for each event is very difficult. Hence, the approach has been to gather more data for the angular particles, in order to provide a more representative selection of the possible combinations of particle shape and orientation.

In short, the experimental data suggest that (on average) the induction period for attachment is reduced in the case of angular particles, and is also reduced at greater approach velocities. The dependence on polar angle *seems* weaker, but still suggests a reduction in induction period for particles that impinge further from the apex (*i.e.* at larger polar angles), in accordance with predictions from numerical modelling (Verrelli *et al.*, 2012).

It should be noted that the apparent dependence of induction period on approach velocity is not linked to the particle size, as might have been thought. In the experiments, the particles fall under the action of gravity, and it is known that larger particles (of the same shape and density), will fall faster. However, analysis of the data indicates that in the present set-up, variations in the approach velocity are predominantly due to the influence of other particles — *i.e.* swarm effects (Verrelli *et al.*, 2012).

Viewing individual scatterplots in isolation may not give a complete picture of the correlation if the parameter of interest depends on multiple variables (Montgomery, Peck and Vining, 2001: 84f.). Hence, to assess the various proposed dependencies simultaneously we undertake multiple nonlinear regression, which permits a

clearer evaluation of the importance of each explanatory variable. For this analysis data from all runs are combined.

Regression

Regressions for each combination of terms produced varying levels of fit. **Table 1** gives the best choice of coefficients — corresponding to the smallest MSE — in equation 1 for increasing numbers of included terms. There is little benefit in introducing more than 4 coefficients, and indeed 3 coefficients is sufficient to capture the influence of each of the three main effects under consideration. The estimated coefficients are generally found to be statistically significant; the only notable exception is for the case of 3 retained terms.

The most important influence on induction time, statistically speaking, is the polar angle, for which an increasing trend with φ^2 is consistently found; β_7 is consistently estimated equal to approximately 0.1. This dependence accords with our previous numerical modelling (Verrelli *et al.*, 2012). It does not appear to be described elsewhere in the literature. The difference between φ^2 and $\cos(\varphi)$ is small, as $\cos(\varphi) - 1$ is directly proportional to φ^2 for small φ. The φ^2 term does not have an obvious physical interpretation, while the $\cos(\varphi)$ term does.

The next-most important influence is the particle shape. In all cases the frit is estimated to have induction periods that are only a few percent of the equivalent spheres, although the precise values fluctuate. This is in agreement with more general studies comparing 'floatability' of angular and round particles, as discussed earlier.

Finally the influence of approach velocity is introduced. Although the $1/v_0^{10}$ term is a good fit for the frit data, there is no obvious physical reason for such an unusual dependence. If this term is disallowed, the penalty is not too great, and the regression is then optimised by including a $1/v_0^2$ term, which is related to the initial kinetic energy of the falling particle. (The term does not fully account for the energy, as this would require the particle mass, which is especially difficult to determine for the angular frit particles.) Although separate models exist relating probability of attachment to the induction period (Yoon and Luttrell, 1989; Nguyen and Schulze, 2004: 265,268) and kinetic energy (Luttrell and Yoon, 1992), it is not clear from these models how the induction period should depend upon kinetic energy.

In all cases the regression predicts increase in τ with increasing $1/v_0$: the slower the particles approach, the longer the induction period. This is conceptually consistent with models of particle–bubble attachment in which the two bodies need to overcome an 'energy barrier' in order for attachment to occur (Luttrell and Yoon, 1992). The hydrodynamically-based models of induction period (see Nguyen and Schulze, 2004: 507ff.) tend to suggest dependence on $1/v_0$; this is still compatible with the overall trend observed presently — the data do not allow a precise judgement of the best exponent. Similarly, the experimental data of Gu *et al.* (2003) for a particle-pickup device is best fit by an equation of the form

$$t_{50\%\,\text{attach}} = \alpha_1 \frac{1}{v_a^{1.14}} + \alpha_2 . \qquad (2)$$

In this device the bubble is squashed against a bed of particles, approaching at a speed v_a, and the kinetics may be quite different to the more natural motions in the present system.

The constant term, β_9, is not needed to describe our data.

CONCLUSIONS

In the literature a number of papers have suggested increasing floatability of more angular (or rougher) particles. A few studies have judged this by flotation recovery, but have not been able to quantify the induction period directly. In the present work we have been able to observe particle–bubble interactions, and thus directly obtain estimates of induction period.

Statistical analysis indicated that the induction period, τ, depended on three parameters. In order of decreasing statistical significance, these are: the polar angle of sliding commencement, φ, an "indicator variable", f, (equal to 1 for frit and 0 for spheres), and the approach velocity, v_0. The suggested fit to the data is:

$$\tau = \left[\left(\frac{73.8\,\text{mm/s}}{v_0} \right)^2 + \left(\frac{\varphi}{3.11^\circ} \right)^2 \right] \left(0.0792 f + (1-f) \right) \quad \text{milliseconds} . \tag{3}$$

Equation 3 indicates that the induction period is reduced for angular particles, high-velocity particles, and particles impinging nearest the apex of the bubble.

Particle shape depends in part on the milling process. The results presented herein indicate the level of attention that should be paid to the *shape* of particles obtained from the grinding operation, besides particle *size*. It may be anticipated that the more angular the particle, the lower the induction period. An extension of the present work would be to measure the effect of different degrees of angularity on the induction period.

ACKNOWLEDGEMENTS

We gratefully acknowledge the assistance of numerous colleagues who assisted with sample preparation (Cathy Edwards), chemical analysis (Cheryl McHugh & team) and microscopy (Matthew Glenn), or advised on other aspects. Funding for this project was provided from CSIRO's Process Science and Engineering Capability Development Fund.

REFERENCES

Ahmed, M M, 2010. Effect of comminution on particle shape and surface roughness and their relation to flotation process, *International Journal of Mineral Processing*, 94(3–4):180–191.

Albijanic, B, Ozdemir, O, Nguyen, A V and Bradshaw, D, 2010. A review of induction and attachment times of wetting thin films between air bubbles and particles and its relevance in the separation of particles by flotation, *Advances in Colloid and Interface Science*, 159(1):1–21.

Anfruns, J F and Kitchener, J A, 1977. Rate of capture of small particles in flotation, *Transactions of the Institute of Mining and Metallurgy*, 86:C9–C15.

Austin, L G and Rogers, R S C, 1985. Powder technology in industrial size reduction, *Powder Technology*, 42(1):91–109.

Bruckard, W J, Sparrow, G J and Woodcock, J T, 2011. A review of the effects of the grinding environment on the flotation of copper sulphides, *International Journal of Mineral Processing*, 100(1–2):1–13.

Brunauer, S, Emmett, P H and Teller, E, 1938. Adsorption of gases in multimolecular layers, *Journal of the American Chemical Society*, 60(2):309–319.

Chan, D Y C, Klaseboer, E and Manica, R, 2011. Film drainage and coalescence between deformable drops and bubbles, *Soft Matter*, 7(6):2235–2264.

Dippenaar, A, 1982. The destabilization of froth by solids. I. The mechanism of film rupture, *International Journal of Mineral Processing*, 9(1):1–14.

Feng, D and Aldrich, C, 2000. A comparison of the flotation of ore from the Merensky Reef after wet and dry grinding, *International Journal of Mineral Processing*, 60(2):115-129.

Forssberg, E, Sundberg, S and Hongxin, Z, 1988. Influence of different grinding methods on floatability, *International Journal of Mineral Processing*, 22(1–4):183-192.

Franks, G V and Gan, Y, 2007. Charging behavior at the alumina–water interface and implications for ceramic processing, *Journal of the American Ceramic Society*, 90(11):3373–3388.

Gaudin, A M, 1926. An investigation of crushing phenomena, *Transactions of the American Institute of Mining and Metallurgical Engineers*, LXXIII:253–316.

Gu, G, Xu, Z, Nandakumar, K and Masliyah, J, 2003. Effects of physical environment on induction time of air–bitumen attachment, *International Journal of Mineral Processing*, 69(1–4):235–250.

Holt, C B, 1981. The shape of particles produced by comminution. A review, *Powder Technology*, 28(1):59–63.

Huh, C and Mason, S G, 1974. The flotation of axisymmetric particles at horizontal liquid interfaces, *Journal of Colloid and Interface Science*, 47(2):271–289.

Husemann, K, Bernhardt, C and Heegn, H, 1976. Feinmahlung und mechanische aktivierung von eisenpulver, *Powder Technology*, 14(1):41–49 (in German).

Koh, P T L, Hao, F P, Smith, L K, Chau, T T and Bruckard, W J, 2009. The effect of particle shape and hydrophobicity in flotation, *International Journal of Mineral Processing*, 93(2):128–134.

Krasowska, M, Krastev, R, Rogalski, M and Malysa, K, 2007. Air-facilitated three-phase contact formation at hydrophobic solid surfaces under dynamic conditions, *Langmuir*, 23(2):549–557.

Kursun, H and Ulusoy, U, 2006. Influence of shape characteristics of talc mineral on the column flotation behavior, *International Journal of Mineral Processing*, 78(4):262–268.

Luttrell, G H and Yoon, R H, 1992. A hydrodynamic model for bubble–particle attachment, *Journal of Colloid and Interface Science*, 154(1):129–137.

Montgomery, D C, Peck, E A and Vining, G G, 2001. *Introduction to Linear Regression Analysis*, Third Edition. (John Wiley & Sons: New York).

Morris, G, Neethling, S J and Cilliers, J J, 2011. An investigation of the stable orientations of orthorhombic particles in a thin film and their effect on its critical failure pressure, *Journal of Colloid and Interface Science*, 361(1):370–380.

Nguyen, A V and Schulze, H J, 2004. *Colloidal Science of Flotation*. (Marcel Dekker: New York, U.S.A.).

Ofori-Sarpong, G and Amankwah, R K, 2011. Comminution environment and gold particle morphology: Effects on gravity concentration, *Minerals Engineering*, 24(6):590–592.

Oliver, J F and Mason, S G, 1977. Microspreading studies on rough surfaces by scanning electron microscopy, *Journal of Colloid and Interface Science*, 60(3):480–487.

Schulze, H J, 1984. *Physico-Chemical Elementary Processes in Flotation : An Analysis from the Point of View of Colloid Science including Process Engineering Considerations*. (Elsevier: Amsterdam, The Netherlands).

Sven-Nilsson, I, 1934. Einfluß der Berührungszeit zwischen Mineral und Luftblase bei der Flotation, *Kolloid Zeitschrift*, 69(2):230–232 (in German).

Verrelli, D I and Koh, P T L, 2010. Understanding particle–bubble attachment: experiments to improve flotation modelling, in *Chemeca 2010*. (IChemE in Australia / EA / RACI / SCENZ-IChemE N.Z.: Adelaide, Australia).

Verrelli, D I, Koh, P T L, Bruckard, W J and Schwarz, M P, 2012. Variations in the induction period for particle-bubble attachment, *Minerals Engineering*, accepted March 2012.

Verrelli, D I, Koh, P T L and Nguyen, A V, 2011. Particle–bubble interaction and attachment in flotation, *Chemical Engineering Science*, 66(23):5910–5921 & Supplementary Material.

Wadell, H, 1935. Volume, shape, and roundness of quartz particles, *The Journal of Geology*, 43(3):250–280.

Yekeler, M, Ulusoy, U and Hiçyılmaz, C, 2004. Effect of particle shape and roughness of talc mineral ground by different mills on the wettability and floatability, *Powder Technology*, 140(1–2):68–78.

Yoon, R-H and Mao, L, 1996. Application of Extended DLVO Theory, IV: Derivation of Flotation Rate Equation from First Principles, *Journal of Colloid and Interface Science*, 181(2):613–626.

Yoon, R H and Luttrell, G H, 1989. The effect of bubble size on fine particle flotation, *Mineral Processing and Extractive Metallurgy Review: An International Journal*, 5(1–4):101–122.

FIGURE CAPTIONS

Figure 1: Schematic of the progress of a particle interacting with and attaching to a bubble (see also Albijanic *et al.*, 2010).

Figure 2: CSIRO Milli-Timer. Adapted from Verrelli *et al*. (2011). The bulb of the pipette is not squeezed.

Figure 3: Micrographs of the particles at various levels of magnification. (A) Spherical particles. (B) Angular frit. Magnifications are (i) 100× (ii) 1000× and (iii) 15000×.

Figure 4: Specific BET surface area of spherical and angular borosilicate glass. The gas in parentheses indicates the species used for characterisation. The prediction for spheres uses the average of surface areas computed for the two end-points of the respective size class; the prediction for frit is double the value for spheres. The error bars enclose 95 % confidence intervals based on the linear regression used in the BET technique.

Figure 5: Induction period for attachment of 75–90 μm borosilicate glass spheres to a 1.56 mm air bubble, as a function of (a) polar angle (Verrelli *et al.*, 2012) and (b) approach velocity.

Figure 6: Induction period for attachment of 75–90 μm borosilicate glass frit to a 1.56 mm air bubble, as a function of (a) polar angle and (b) approach velocity.

TABLE CAPTIONS

Table 1: Optimal regressions of τ on combinations of the candidate variables, using equation 1 with 1–4 coefficients. (For 3′, the $1/v_0^{10}$ term is disallowed: β_1 is set to 0.) The uncertainties indicate the 95 % confidence intervals. Values in red italics are subject to high uncertainty.

FIGURES

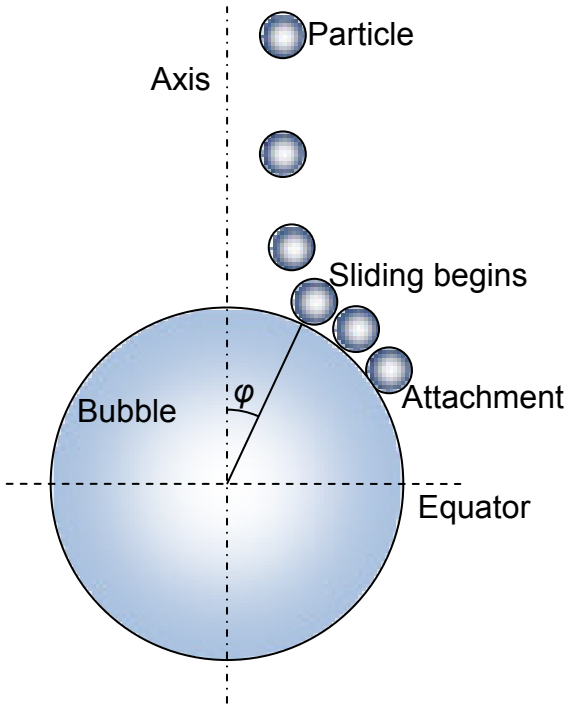

Figure 1: Schematic of the progress of a particle interacting with and attaching to a bubble (see also Albijanic *et al.*, 2010).

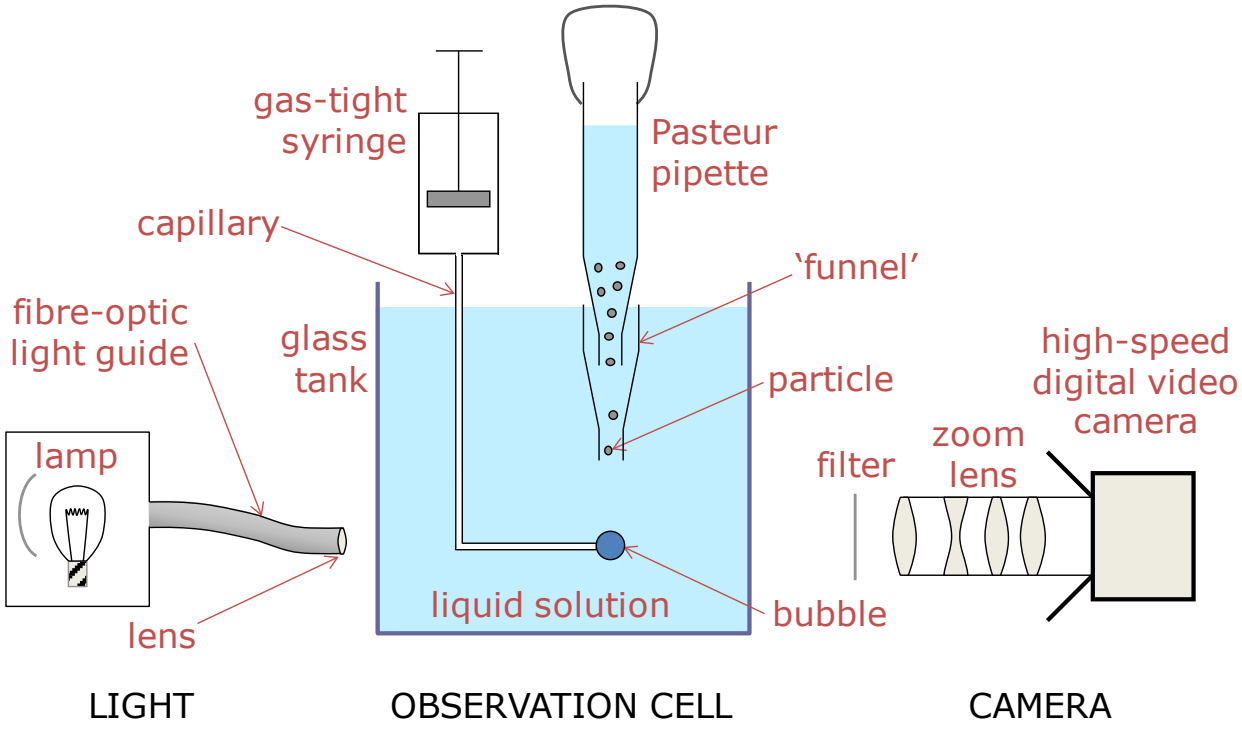

Figure 2: CSIRO Milli-Timer. Adapted from Verrelli *et al.* (2011). The bulb of the pipette is not squeezed.

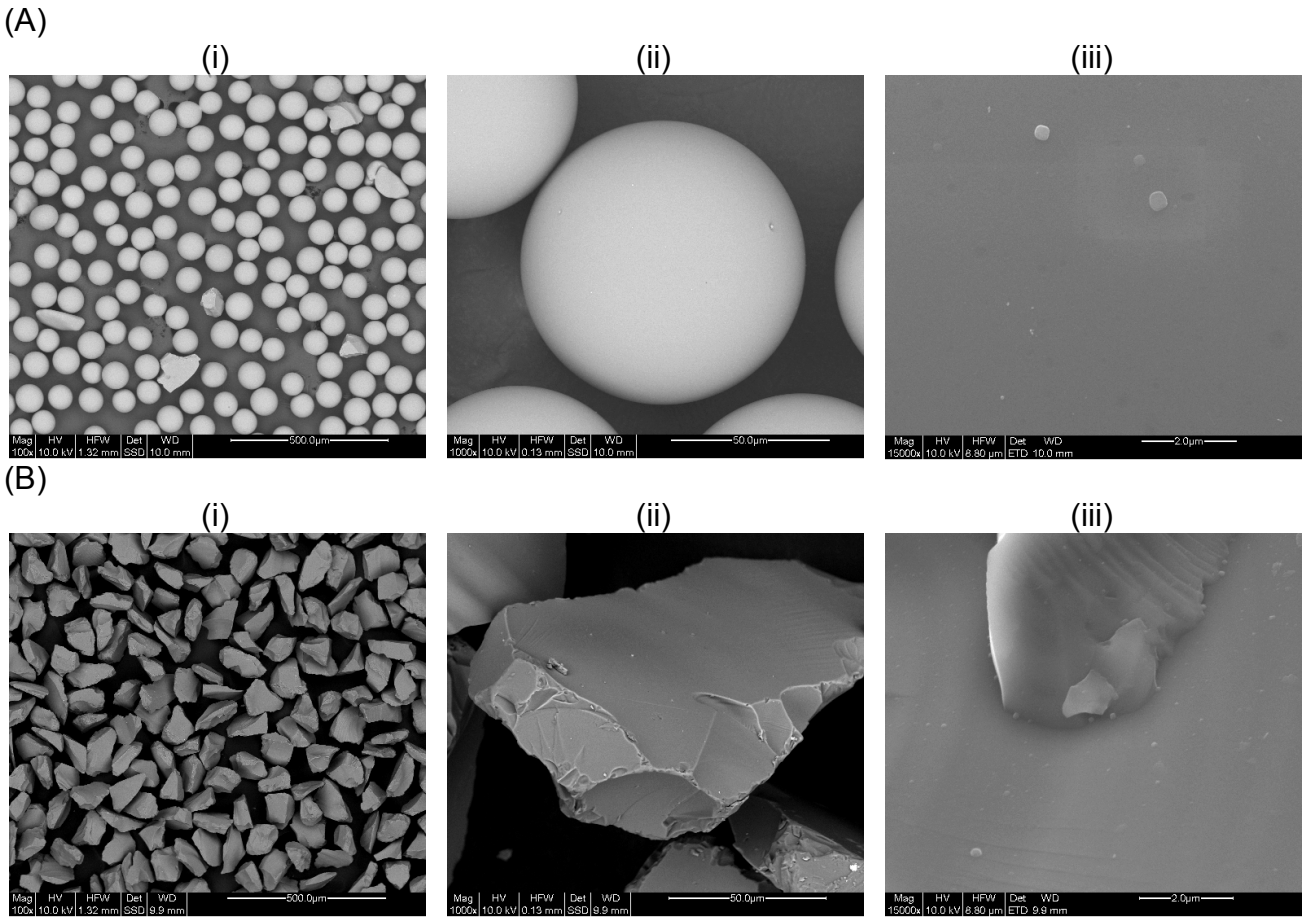

Figure 3: Micrographs of the particles at various levels of magnification. (A) Spherical particles. (B) Angular frit. Magnifications are (i) 100× (ii) 1000× and (iii) 15000×.

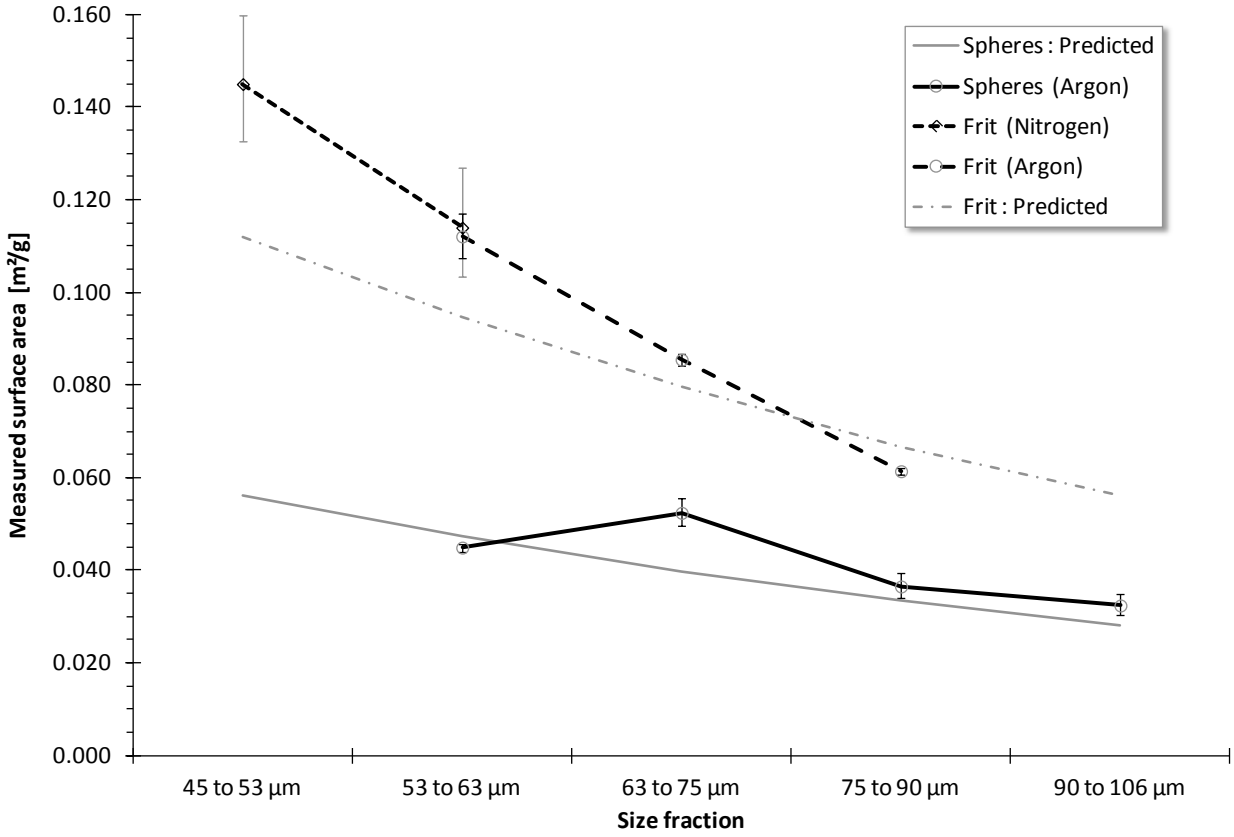

Figure 4: Specific BET surface area of spherical and angular borosilicate glass. The gas in parentheses indicates the species used for characterisation. The prediction for spheres uses the average of surface areas computed for the two end-points of the respective size class; the prediction for frit is double the value for spheres. The error bars enclose 95 % confidence intervals based on the linear regression used in the BET technique.

(a)

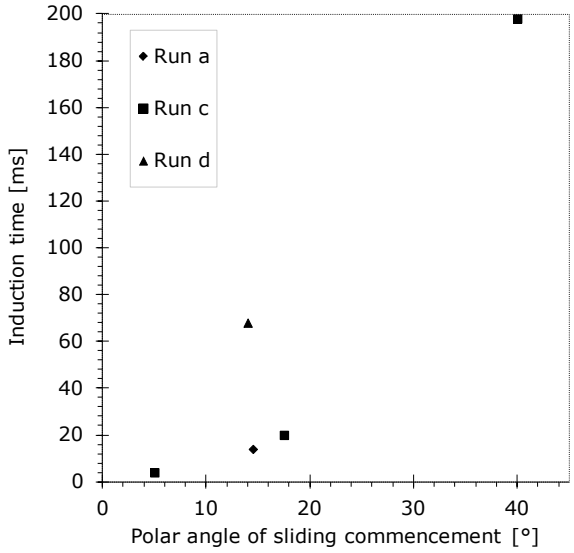

(b)

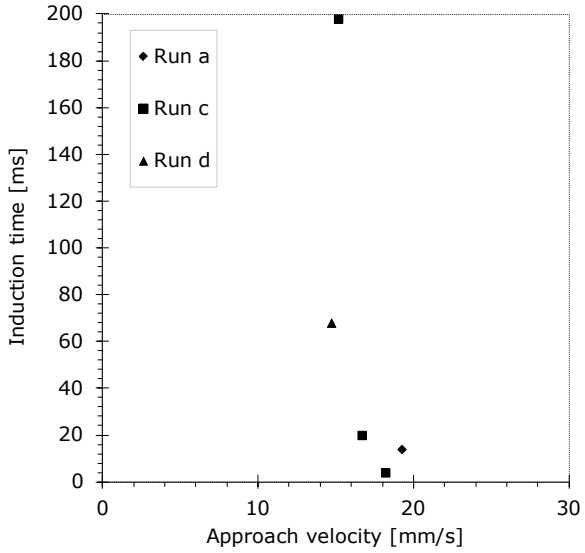

Figure 5: Induction period for attachment of 75–90 µm borosilicate glass spheres to a 1.56 mm air bubble, as a function of (a) polar angle (Verrelli *et al.*, 2012) and (b) approach velocity.

(a)

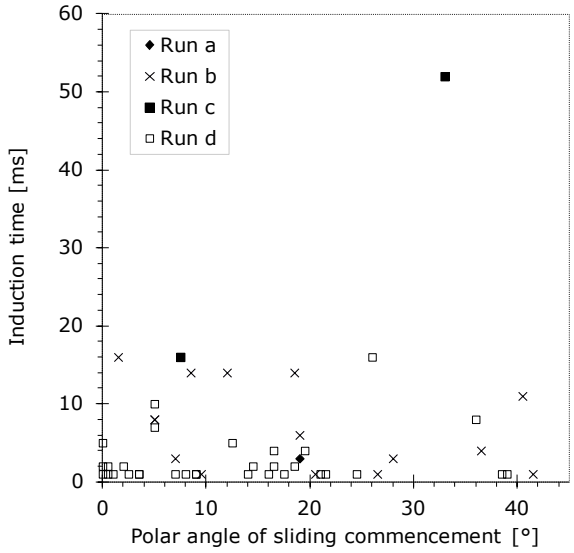

(b)

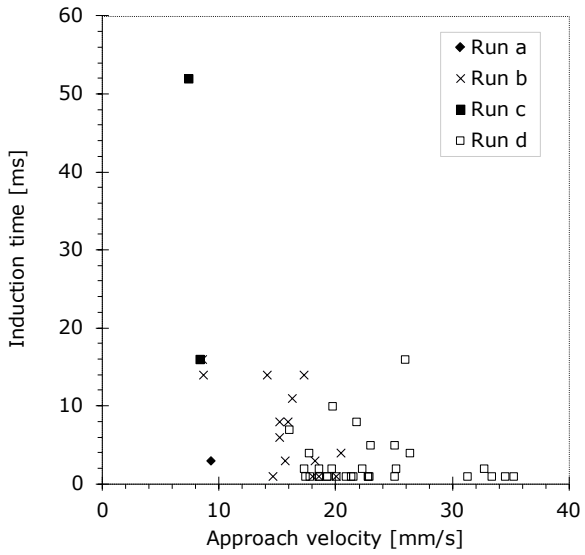

Figure 6: Induction period for attachment of 75–90 µm borosilicate glass frit to a 1.56 mm air bubble, as a function of (a) polar angle and (b) approach velocity.

TABLES

Table 1: Optimal regressions of r on combinations of the candidate variables, using equation 1 with 1–4 coefficients. (For 3′, the $1/v_0^{10}$ term is disallowed: β_1 is set to 0.) The uncertainties indicate the 95 % confidence intervals. Values in red italics are subject to high uncertainty.

Coefficient	Corresponding parameter		Number of coefficients				
			1	2	3	3′	4
β_1	$1/v_0^{10}$	[s^{10}/mm^{10}]			*7.63×10^{11} ± 8.82×10^{11}*		
β_2	$1/v_0^2$	[s^2/mm^2]				5.45×10^3 ± 3.04×10^3	84.3×10^3 ± 6.3×10^3
β_3	$1/v_0$	[s/mm]					
β_4	Approach velocity, v_0	[mm/s]					23.9 ± 3.5
β_5	v_0^2	[mm^2/s^2]					
β_6	Polar angle, φ	[°]					
β_7	φ^2	[$°^2$]	0.0222 ± 0.0117	0.124 ± 0.013	0.123 ± 0.010	0.103 ± 0.016	
β_8	cos(φ)	[–]					−698 ± 76
β_9	constant	[ms]					
β_{10}	Frit flag, f	[–]		0.0569 ± 0.0412	*0.0303 ± 0.0311*	0.0792 ± 0.0362	0.0299 ± 0.0071
MSE		[ms^2]	717.8	116.8	64.2	97.0	39.4